Journal of Nuclear Materials 392 (2009) 213–218

Contents lists available at ScienceDirect

Journal of Nuclear Materials

journal homepage: www.elsevier.com/locate/jnucmat

Effect of coating temperature on properties of the SiC layer in TRISO-coated particles

Weon-Ju Kim *, Jeong Nam Park, Moon Sung Cho, Ji Yeon Park

Nuclear Materials Research Division, Korea Atomic Energy Research Institute, 1045 Daedeok-daero, Yuseong-gu, Daejeon 305-353, Republic of Korea

A B S T R A C T

The effect of coating temperature on properties of the SiC layer in TRISO-coated particles was investigated. An increase in coating temperature resulted in a significant coarsening of surface microstructures and an increase of the pore size and porosity of SiC layers. The SiC layers formed at 1400–1550 °C had nearly stoichiometric compositions whereas the SiC layer formed at 1600 °C contained a small amount of free carbon. The degradation of hardness and elastic modulus of the SiC layers coated at 1550 and 1600 °C was attributed to the increased porosity of the specimens and partly to the existence of free carbon. The fracture stress of the SiC layer measured by the crush test of hemispherical shell specimen did not correlate with the hardness and elastic modulus, and there was no clear dependence of the fracture stress on the coating temperature; this lack of correlation can be explained by the large roughness of the inner surface of the SiC layer.

1. Introduction

TRISO-coated fuel particles for high-temperature gas-cooled reactors consist of UO_2 microspheres coated with layers of porous pyrolytic carbon (porous PyC), inner dense PyC (IPyC), silicon carbide (SiC), and outer dense PyC (OPyC) [1,2]. The porous PyC coating layer, the so-called buffer layer, attenuates fission recoils and provides a void volume for gaseous fission products and carbon monoxide. The IPyC layer acts as containment for gaseous products. The OPyC layer protects the SiC coating layer by inducing a compressive stress along with the IPyC layer and provides chemical compatibility with the graphite matrix in a fuel compact [1]. Among the TRISO coating layers the SiC layer is particularly important because it acts as a diffusion barrier to gaseous and metallic fission products and as a miniature pressure vessel for the particle. In order to insure the integrity of the SiC layer after fabrication and in use, the microstructure, mechanical properties, and chemical composition of the SiC layer should be controlled properly [3].

For uniform coating of the microspherical particles, the TRISO coating is formed using the fluidized-bed chemical vapor deposition (FBCVD) method. Characteristics of the coating layer depend largely on the FBCVD conditions such as the gas flow rate, concentration of the coating gas, coating temperature, etc. [4–11]. Among the deposition parameters, the coating temperature is particularly important to determine the properties of the SiC layer. Minato and Fukuda [6,7] reported that coating temperature was the main parameter affecting the content of free silicon, density, crystallite size, and microstructure. They found that free silicon was co-deposited with β-SiC at temperatures lower than 1400–1500 °C when only hydrogen was used as a fluidizing gas while pure β-SiC was deposited even at 1400 °C when a mixture gas of hydrogen and argon was used. Crystallite size increased and lattice distortion decreased with increasing coating temperature [6]. Stinton and Lackey [10] reported that the density of SiC increased with temperature between 1400 and 1625 °C and decreased at higher temperatures. They also reported that the crushing strength of SiC-coated particles decreased with increasing coating temperature and the strength could be correlated with the grain size. Xu et al. [11] studied the effect of the coating temperature on the density, microstructure, strength, and Young's modulus of SiC layer at coating temperatures between 1450 and 1650 °C. They found that strength and Young's modulus of SiC were the highest at coating temperatures of 1500–1550 °C and decreased significantly at temperatures lower or higher than the optimum condition.

In this study, we investigated the effect of the coating temperature on the properties of the SiC layer while fixing other deposition parameters. Microstructure, chemical composition, porosity, and mechanical properties of the SiC layers coated at different temperatures were characterized by various techniques.

2. Experimental procedure

2.1. Fabrication of coated particles

Coating of the TRISO particles was conducted using ZrO_2 kernels as surrogates for UO_2 particles in a FBCVD reactor. In this work, a graphite tube of 25 mm inner diameter with an inlet nozzle of 3 mm at the base of a 60° cone was used as a coating bed. At the deposition temperatures, ZrO_2 particles were put into the coater

* Corresponding author. Tel.: +82 42 868 8029; fax: +82 42 868 8549.
E-mail address: weonjkim@kaeri.re.kr (W.-J. Kim).

0022-3115/$ - see front matter © 2009 Elsevier B.V. All rights reserved.
doi:10.1016/j.jnucmat.2009.03.012

from the top of the graphite tube in the presence of an Ar flow from the bottom of the coater. After assuring the fluidization of the particles by viewing through a quartz window, reactants were put into the coater to produce a coating layer on the particles. Input gases for the depositions of the buffer, IPyC (OPyC) and SiC were C_2H_2/Ar, C_2H_2/C_3H_6/Ar, and CH_3SiCl_3 (MTS)/H_2/Ar, respectively. For the deposition of the SiC layer, the coating temperature was varied between 1400 and 1600 °C at a constant gas flow rate and an input gas ratio ((Ar + H_2)/MTS) of 100. Coating thicknesses of the SiC layers were controlled in the range of 34–40 μm by varying coating times. All the TRISO layers were continuously coated without unloading the particles between coating steps.

2.2. Characterization methods

Microstructures of the SiC layer were characterized using optical microscopy (OM) and scanning electron microscopy (SEM). For observation of the outer surface of the SiC layer, the OPyC layer was burned off at 800 °C for 2 h in air. Phase purity and stoichiometry of the SiC layer were measured using X-ray powder diffraction (XRD) and Auger electron spectroscopy (AES), respectively. The XRD was carried out after burning off the OPyC layer. The AES analysis was performed on the polished cross-sections of the coated particles. The native oxide layer on the SiC surface was sputtered using an Ar ion beam before the analysis. Pore size distribution and porosity of the SiC layer were measured from 20 SEM micrographs for each specimen using an image analyzer. Hardness and elastic modulus were evaluated by a nano-indentation tester (NanoIndenter XP, MTS) equipped with a Berkovich diamond tip. Indentations were applied along the middle plane of the SiC layer on the diamond-polished cross-section to exclude interference of the adjacent IPyC and OPyC layers. Five particles were measured for each coating condition and 10 indentations were made for each particle.

The fracture stress of the SiC layer was measured through a crush test of a hemispherical shell specimen which was a similar configuration to the report by Hong et al. [12]. The TRISO-coated particles mounted in an epoxy resin were ground close to the equatorial plane of the particles and the SiC hemispherical shell specimens were collected after burning off the IPyC and OPyC layers. The hemispherical shell specimen laid on an alumina plate was loaded by an upper alumina rod. The crosshead speed used was 0.1 mm/min. The fracture stress of the SiC hemispherical shell specimen was calculated from the critical load for the cracking of the shell. Finite element (FE) analysis was used to derive a semi-empirical equation for the stress calculation and the detailed procedure is given elsewhere [13]. In brief, the FE analysis was performed using a commercial program, ABAQUS. In the analysis, the FE mesh for the hemispherical shell, upper and lower alumina blocks was set with eight-node bilinear axi-symmetric quadrilateral element. The entire system consists of approximately 50000 elements and 50000 nodes. The contacts between the hemispherical shell, upper and lower alumina blocks are assumed to be frictionless. It is also assumed that there is a point contact between the SiC shell and upper alumina rod. The fracture load–stress relationship obtained through the FE analysis is given by:

$$\sigma_f = \frac{1}{t^2} \times \frac{E^*}{(\alpha + E^*)} \times P_f, \tag{1}$$

$$\frac{1}{E^*} = \frac{1}{E_{SiC}} + \frac{1}{E_{indenter}}, \tag{2}$$

where σ_f, t, P_f, α (=13.21), E_{SiC} (=450 GPa), and $E_{indenter}$ (=300 GPa) are the fracture stress, the thickness of the SiC shell, the fracture load, the dimensionless parameter, and the elastic moduli of SiC and alumina indenter, respectively. Statistical analysis of the fracture stress was also performed by the two-parameter Weibull analysis. More than 80 samples were used for the Weibull analysis.

3. Results and discussion

We fabricated TRISO-coated particles with variation of coating temperature for the SiC layer while fixing coating conditions for the buffer, IPyC and OPyC layers. The inner radii of the SiC layers were about 390 μm and the thickness was also kept as constant as possible, between 34 and 40 μm. Typical SEM and optical micrographs of the fabricated TRISO particles are shown in Fig. 1. Fig. 2 shows XRD patterns of the coated particles after burning off the OPyC layers. There is no appreciable difference in the XRD results with variation of the coating temperature. The SiC layers formed at various temperatures consists exclusively of the β-SiC phase, at least within the resolution limit of the XRD technique, except for the specimen coated at 1600 °C. The small carbon peaks were due to the IPyC layer beneath the SiC layer while a small amount of free carbon was co-deposited with the β-SiC in case of the 1600 °C specimen, judged from the AES results of Fig. 3. The stoichiometry of the SiC layer was analyzed by the AES method. It can be seen from Fig. 3 that stoichiometric SiC is obtained at coating temperatures below 1550 °C while excess carbon appears at 1600 °C. The co-deposition of carbon at high temperatures is expected from thermodynamic calculations [14,15] and is consistent with a previous report in which the β-SiC + C phases tended to be deposited at high temperatures [16].

Fig. 4 shows deposition rate of the SiC layer as a function of coating temperature. The deposition rate tends to increase with increasing coating temperature, within the temperature range studied in this work, although the temperature dependence of

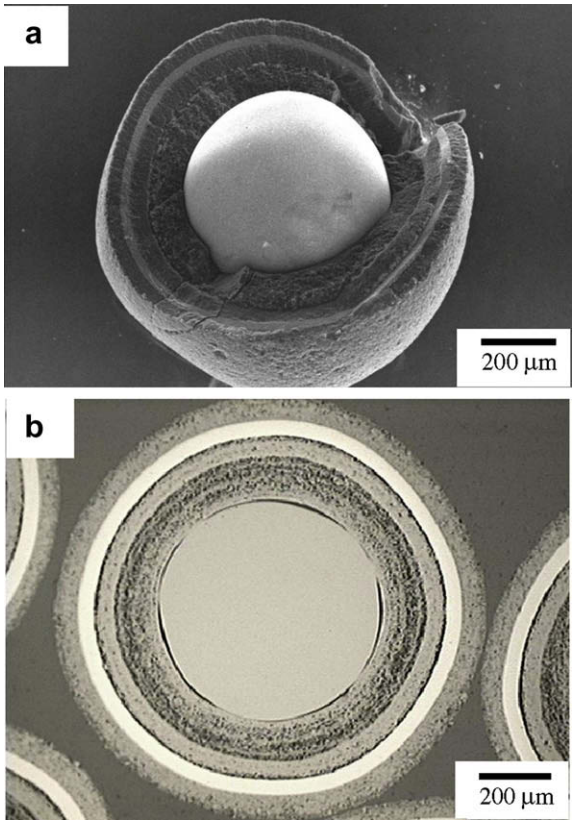

Fig. 1. Typical SEM (a) and optical micrographs (b) of the TRISO-coated particles fabricated in this study.

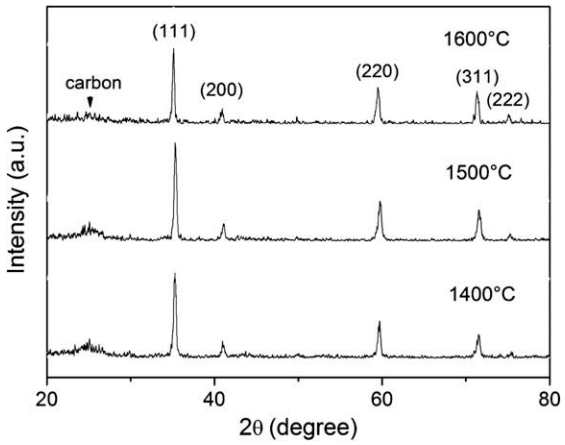

Fig. 2. XRD patterns of the SiC layers coated at different temperatures.

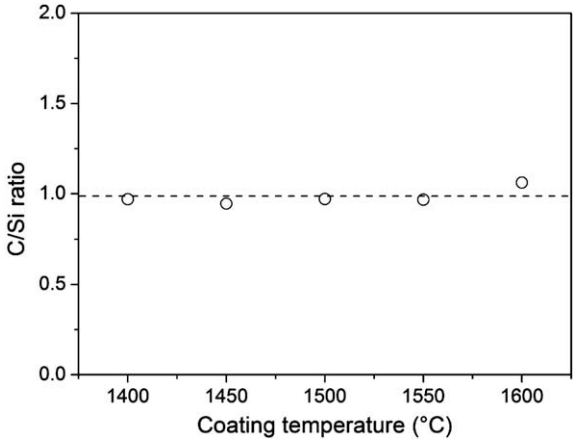

Fig. 3. Results of AES analyses for the SiC layers coated at different temperatures.

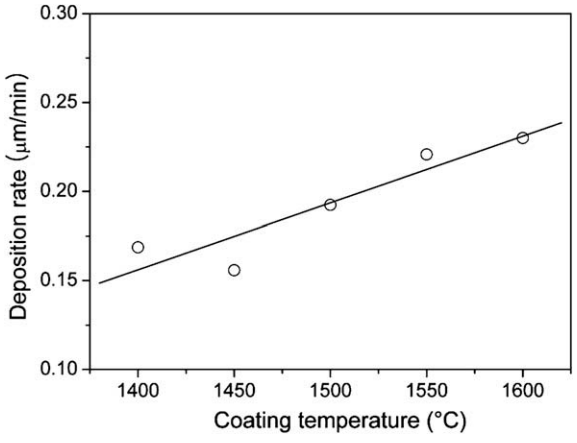

Fig. 4. Deposition rate of the SiC layer as a function of coating temperature.

the deposition rate is low. The activation energy of the deposition reaction calculated from the slope of an Arrhenius plot, not shown here, was 11.9 kcal/mol. This relatively low activation energy suggests that the mass transport mechanism is the rate-controlling step of the SiC deposition reaction [17], which is consistent with the interpretation in a previous report [7]. Fig. 5 shows the outer surface microstructures of the SiC layer coated at 1400, 1500, and 1600 °C. The outer surface of the SiC layer has a high roughness

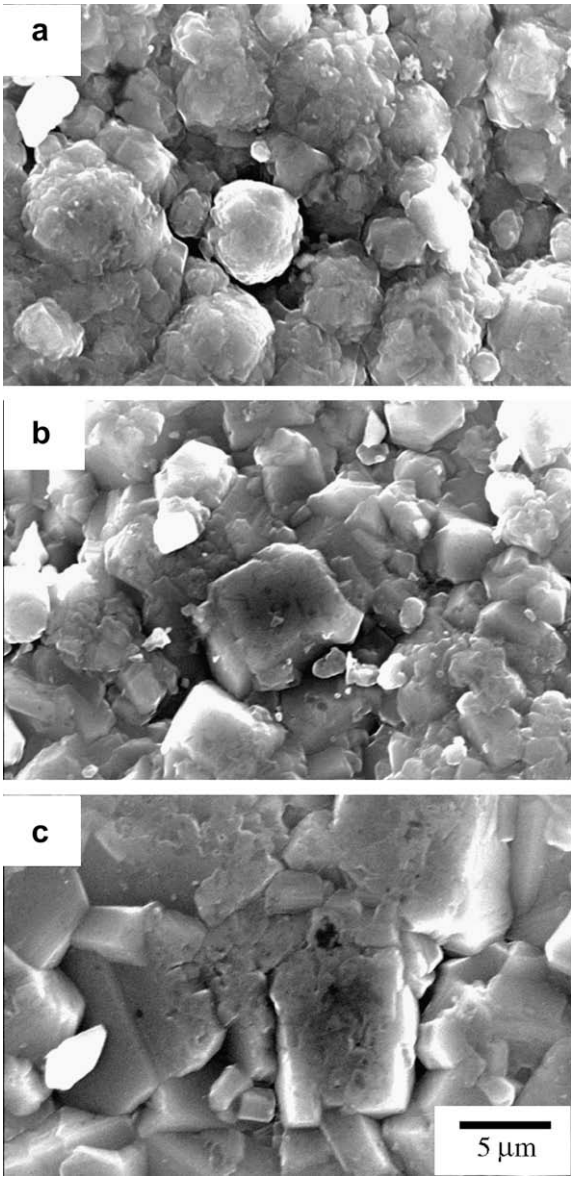

Fig. 5. SEM microstructures for the outer surfaces of the SiC layers coated at 1400 (a), 1500 (b), and 1600 °C (c).

irrespective of the coating temperature. At the coating temperature of 1400 °C, the SiC surface consists of pebble-like deposits, being agglomerated with small faceted grains. As the coating temperature increases the grains become more faceted and the grain size increases significantly.

Pore size distribution and porosity of the SiC layers coated at various temperatures are shown in Figs. 6 and 7, respectively. At coating temperatures below 1500 °C, most pores are less than 1.5 μm in size whereas pores larger than 2.0 μm start to appear at coating temperatures of 1550 and 1600 °C. The porosity also starts to increase at coating temperatures higher than 1500 °C. In addition, the average pore size of the SiC layers, not shown here, asymptotically increased from 0.29 to 0.45 μm as the coating temperature increased from 1400 to 1600 °C. The increase of the pore size and porosity could be attributed to the increase of the deposition rate and the grain size as previously shown in Figs. 4 and 5. Another possible reason for the porosity increase would be a change in the mode of particle fluidization. At an optimum gas flow rate, the mode of particle fluidization is characterized as normal

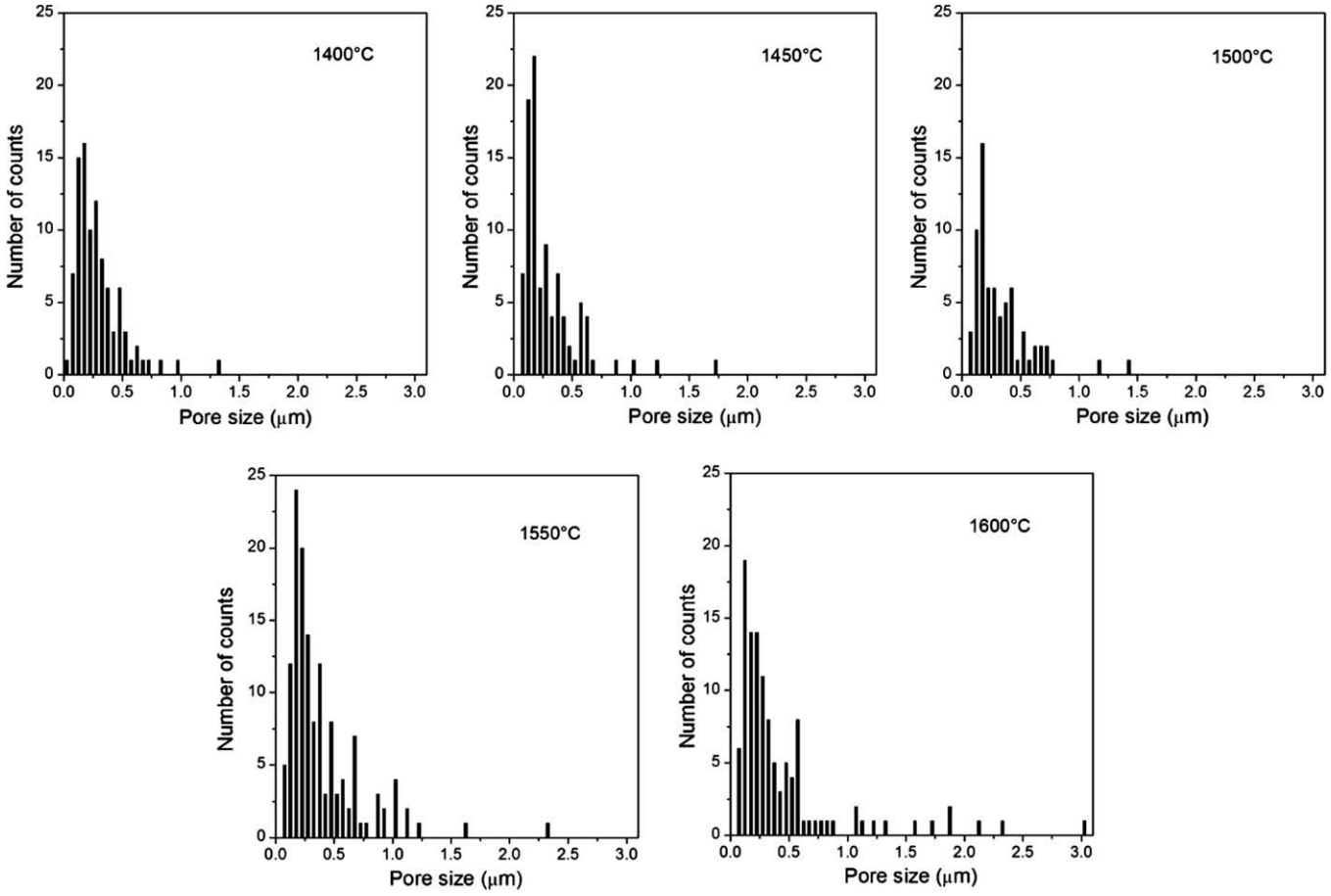

Fig. 6. Pore size distributions in the SiC layers coated at different temperatures.

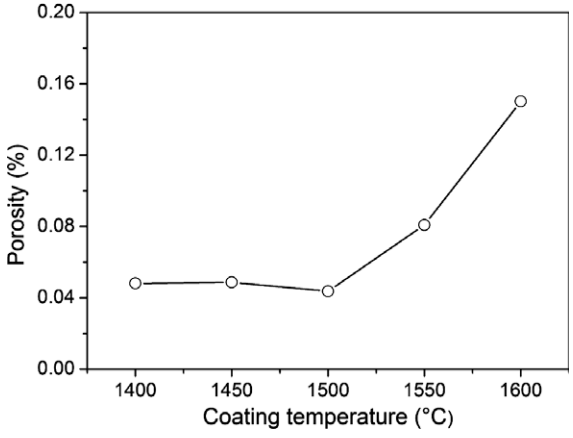

Fig. 7. Variation of the porosity in SiC layers as a function of the coating temperature.

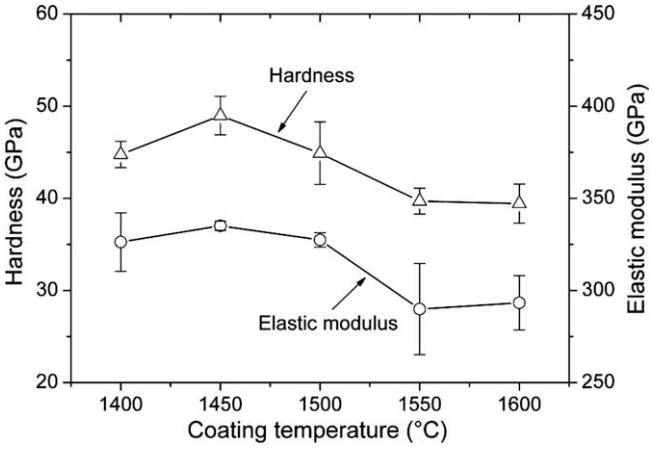

Fig. 8. Hardnesses and elastic moduli of the SiC layers coated at different temperatures.

spouting. That is, a stream of the particles rises rapidly in the center as the spout, reaches a maximum level, then falls back onto the annular space around the spout and travels downward uniformly as a packed bed [18,19]. As the coating temperature increases, while other coating parameters such as the gas flow rate, the amount of loaded particles, the configuration of the gas distributor, etc. are held constant, the particles can be fluidized more vigorously due to an increase of the viscosity of input gases. If the particle fluidization is in the violent mode, the particles will be blown out of the normal deposition zone and the probability of the formation of internal flaws will increase [18], leading to an increase of the pore size and porosity of the SiC layer.

Fig. 8 shows hardnesses and elastic moduli of the SiC layers measured by the nano-indentation method. Although the hardness and the elastic modulus reveal maxima at the coating temperature of 1450 °C, the differences are not significant in the temperature range 1400–1500 °C. At coating temperatures of 1550 and 1600 °C, however, the SiC layers reveal an appreciable degradation of both the hardness and the elastic modulus. The decrease of the

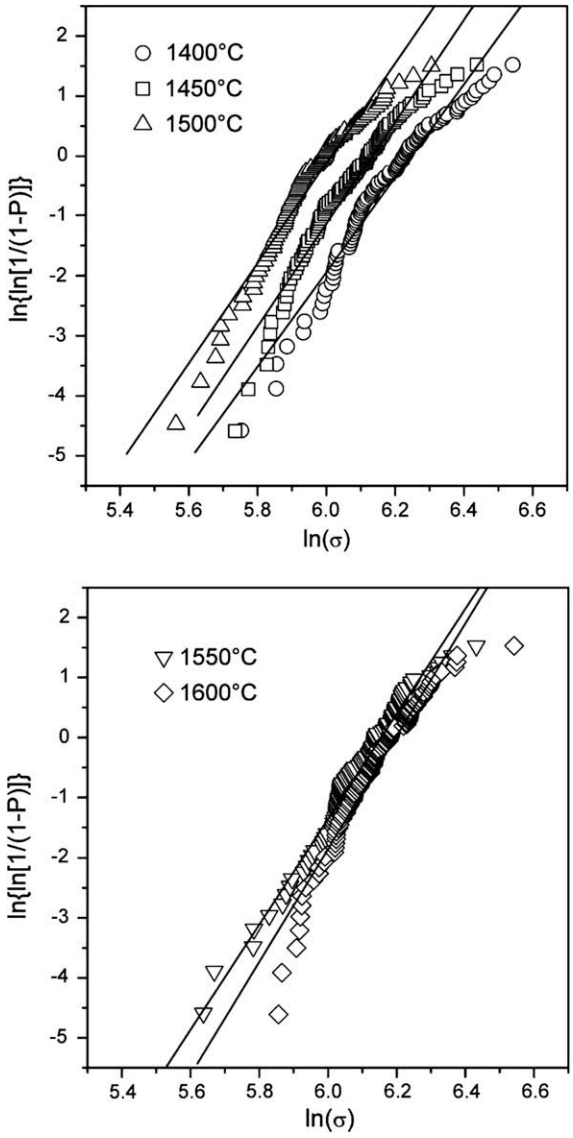

Fig. 9. Weibull plots for the fracture stresses of the SiC layers coated at different temperatures. The data are displayed in two graphs for clarity.

hardness and elastic modulus are mainly due to the increase of the porosity and partly to the existence of free carbon, especially in case of the 1600 °C specimen.

Weibull plots and a summary of statistical parameters for the fracture stresses measured by the crush test of hemispherical shell specimens are depicted in Fig. 9 and Table 1, respectively. The effective surface appeared in the last column of Table 1 indicates the surface area to which a uniform stress is subjected. The effective surface area was calculated from the tensile stress distribution at the inner surface of the shell specimen in the FE analysis by assuming a point contact between the SiC shell and upper alumina rod. As pointed out by Hong et al. [12], however, there is a significant surface roughness-induced flattening at the contact between the shell and upper loading block. The contact flattening has large influence on the effective surface and thus on the determination of fracture stress. Therefore, the fracture stress data shown in this study should be regarded only as relative values between different coating temperatures. As shown in Table 1, the mean fracture stresses do not show a wide variation with varying coating temperatures although the 1500 °C specimen has a slightly lower stress. Weibull moduli also reveal similar values between 7.9 and 9.4. The results of the fracture stress tests do not correlate with the nano-indentation results in Fig. 8 and there is no clear dependence of the fracture stress on the coating temperature. These results can be interpreted as follows. The fracture of the SiC hemispherical shell specimen is initiated at the inner surface with a high roughness of several micrometers in size, which originated from the uneven outer surface of the IPyC layer, and the roughness is at a larger scale than the pore size in the SiC layer, as shown in Fig. 10. Therefore, it is likely that the fracture stress is dominated by the roughness of the SiC inner surface, thus overshadowing the effects of the internal porosity and microstructural differences on the fracture stress. The effect of the surface roughness on the fracture strength of the SiC layer in TRISO-coated particles has been pointed out by several researchers [16,20]. Evans et al. [20] measured the flexural strengths of the outer and the inner surface layers of the SiC coatings using hemispherical shell specimens. They observed that the inner surface strength increased from 720 to 1350 MPa and the outer surface strength from 620 to 2500 MPa with decreasing surface roughness. Ford et al. [16] also reported that the internal structural variations did not affect the median strength of SiC coatings although variations in strength could be achieved by alteration of the surface roughness of SiC coatings. Another aspect to be considered, however, is that the roughness of the IPyC/SiC interface may be beneficial in increasing the debonding strength of the interface. A higher interfacial strength can minimize localized debonding of the IPyC/SiC interface and avoid stress concentration in the SiC layer, leading to a lower failure fraction of particles [21].

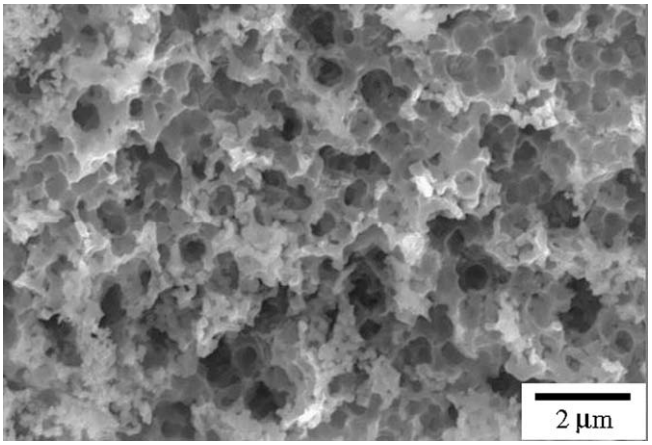

Fig. 10. A typical SEM microstructure for the inner surface of the SiC layer coated at 1550 °C.

Table 1
Summary of fracture stress tests of SiC hemispherical shell specimens.

Coating temperature (°C)	Number of specimens	Mean stress σ_m (MPa)	Coefficient of variation (%)	Weibull modulus	Effective surface area ($\times 10^{-4}$ mm^2)
1400	97	517	14.2	7.9	5.15
1450	98	464	13.1	8.3	4.20
1500	87	409	13.4	8.3	3.34
1550	98	471	12.5	8.8	4.00
1600	100	491	12.0	9.4	3.20

4. Conclusions

We investigated the effect of coating temperature on the microstructure, chemical composition, porosity, and mechanical properties of the SiC layer in TRISO-coated particles. The kinetics of the SiC coating reaction appeared to be controlled by diffusion through the gas phase boundary. The SiC layers coated at 1400–1550 °C had nearly stoichiometric compositions whereas the SiC layer coated at 1600 °C contained a small amount of free carbon. The pore size and porosity of the SiC layer increased with increasing coating temperature, especially at 1550 and 1600 °C. An appreciable degradation of the nano-indentation hardness and elastic modulus resulted for the SiC layers coated at 1550 and 1600 °C, which could be attributed mainly to the increased porosity of the specimens and partly to the existence of free carbon in the 1600 °C specimen. The fracture stress measured by crushing hemispherical shell specimens did not reveal a clear dependence on the coating temperature. This could be attributed to the large roughness of the inner surface of the SiC hemispherical shells in which the surface roughness acted as a site for fracture origin and overshadowed the porosity and microstructure effects in determining the fracture stress.

Acknowledgements

This work was financially supported by Ministry of Education, Science and Technology (MEST) through the Nuclear Hydrogen Technology Development (NHTD) program. The authors would like to thank Mr H.K. Lee for FE analyses.

References

[1] H. Nabielek, W. Kühnlein, W. Schenk, W. Heit, A. Christ, H. Ragoss, Nucl. Eng. Des. 121 (1990) 199.
[2] J. Chang, Y.-W. Kim, K.-Y. Lee, Y.-W. Lee, W.J. Lee, J.-M. Noh, M.-H. Kim, H.-S. Lim, Y.-J. Shin, K.-K. Bae, K.-D. Jung, Nucl. Eng. Technol. 39 (2007) 111.
[3] K. Minato, H. Kikuchi, K. Fukuda, N. Suzuki, H. Tomimoto, N. Kitamura, M. Kaneko, Nucl. Technol. 111 (1995) 260.
[4] N. Piccinini, in: E.J. Henly, J. Lewins (Eds.), Advances in Nuclear Science and Technology, vol. 8, Academic Press, New York, 1975, p. 256.
[5] J.H. Park, W.-J. Kim, J.N. Park, K.H. Park, J.Y. Park, Y.W. Lee, Kor. J. Mater. Res. 17 (2007) 160.
[6] K. Minato, K. Fukuda, J. Mater. Sci. 23 (1988) 699.
[7] K. Minato, K. Fukuda, J. Nucl. Mater. 149 (1987) 233.
[8] T.D. Gulden, J. Am. Ceram. Soc. 51 (1968) 424.
[9] J.R.C. Gough, D. Kern, J. Nucl. Energy 21 (1967) 623.
[10] D.P. Stinton, W.J. Lackey, Am. Ceram. Soc. Bull. 57 (1978) 568.
[11] S.J. Xu, J.G. Zhou, B. Yang, B.Z. Zhang, J. Nucl. Mater. 224 (1995) 12.
[12] S.-G. Hong, T.-S. Byun, R.A. Lowden, L.L. Snead, Y. Katoh, J. Am. Ceram. Soc. 90 (2007) 184.
[13] H.K. Lee, D.K. Kim, J. Kor. Ceram. Soc. 44 (2007) 368.
[14] A.I. Kingon, J.L. Lutz, P. Liaw, R.F. Davis, J. Am. Ceram. Soc. 66 (1983) 558.
[15] M.D. Allendorf, J. Electrochem. Soc. 140 (1993) 747.
[16] L.H. Ford, N.S. Hibbert, D.G. Martin, J. Nucl. Mater. 45 (1972/1973) 139.
[17] M. Ohring, The Materials Science of Thin Films, Academic Press, New York, 1992.
[18] K. Minato, H. Kikuchi, K. Fukuda, N. Suzuki, H. Tomimoto, N. Kitamura, M. Kaneko, Nucl. Technol. 106 (1994) 342.
[19] K.B. Mathur, P.E. Gishler, AIChE J. 1 (1955) 157.
[20] A.G. Evans, C. Padgett, R.W. Davidge, J. Am. Ceram. Soc. 56 (1973) 36.
[21] D.A. Petti, J. Buongiorno, J.T. Maki, R.R. Hobbins, G.K. Miller, Nucl. Eng. Des. 222 (2003) 281.